CRYSTAL GROWTH & DESIGN
2008
VOL. 8, NO. 7
2497–2504

Synthesis of a Se^0/Calcite Composite Using Hydrothermal Carbonation of $Ca(OH)_2$ Coupled to a Complex Selenocystine Fragmentation

G. Montes-Hernandez,*[,†] A. Fernández-Martínez,[†,‡] L. Charlet,[†] F. Renard,[§,||] A. C. Scheinost,[⊥,#] and M. Bueno[▽]

LGIT, University Joseph Fourier, Observatoire de Grenoble and CNRS, BP 53 X, 38420 Grenoble Cedex 9, France, Institute of Radiochemistry, FZD, Dresden, Germany, The Rossendorf Beamline at ESRF, 6 rue Jules Horowitz, BP 220, 38043 Grenoble Cedex, France, LGCA, University Joseph Fourier, Observatoire de Grenoble and CNRS, BP 53 X, 38420 Grenoble Cedex 9, France, Physics of Geological Processes, University of Oslo, Norway, LCABIE, IPREM, UMR CNRS 5254, Université de Pau et des Pays de l'Adour, Hélioparc Pau-Pyrénées, 2 avenue du Président Angot, 64000 Pau, France, and Institut Laue-Langevin, B.P. 156, 38042 Grenoble Cedex 9, France

Received February 5, 2008; Revised Manuscript Received April 4, 2008

ABSTRACT: Elemental selenium (Se^0)/calcite composites were synthesized in a batch system by hydrothermal carbonation of calcium hydroxide under high CO_2−Ar pressure (90 bar) and high temperature (90 °C) coupled to a complex selenocystine fragmentation. Under O_2-poor conditions, the composite consisted predominantly of spherical, amorphous nanoparticles of elemental red selenium (<500 nm) deposited on the calcite matrix. Conversely, under O_2-rich conditions, the composite consisted rod-shaped, well-crystallized microparticles of elemental gray selenium (<25 μm) dispersed in the calcite matrix. The carbonate matrix was constituted by nano- to microrhombohedral crystals (<2 μm) and micrometric agglomerates and/or aggregates (<5 μm). Our results present a new synthesis path to Se^0/calcite composites, with spherical or rod-shaped Se^0 morphology with high potential for medical (e.g., dietary supplement) or industrial (e.g., pigments) applications. Furthermore, this study may have implications in the field of biomineralization.

1. Introduction

Selenium is well-known for its photochemical and semiconductor properties and is used in solar cells, rectifiers, photographic exposure meters and xerography.[1–3] It is also a key trace element required in small quantities in humans and animals for a number of selenium-dependent enzymes, such as glutathione peroxidase (GPX) and thioredoxin reductase; however this element can also be toxic in larger doses. Both the beneficial and toxic effects of selenium are based on doses ingested and on its chemical forms.[4–10] Inorganic and organic selenium compounds have been identified in nature. Selenium can easily form compounds with metals and occurs in about 50 minerals. It is present in four different oxidation states in aqueous and subsurface systems, namely −2, 0, +4 and +6.[11–13] Obviously, the fate and transport of Se in contaminated sites are controlled by its chemical form and speciation.

Recently, elemental selenium nanoparticles have been synthesized through various approaches, such as laser ablation, solution-phase and vapor-phase growth, electrochemical synthesis, photothermally assisted solution phase, ultrasonic, hydrothermal or solvothermal method and micelle-mediated synthesis.[1] Searching and designing novel methods to synthesize elemental selenium with controlled morphology is important both for fundamental issues and for industrial applications. For example, Se^0 nanoparticles are attracting more and more attention due to their excellent high biological activity and lower toxicity in animals and humans.[3]

Calcium carbonate is an inorganic compound that has been widely studied due to its abundance in nature as a mineral and biomineral. Calcium carbonate particles are found in three polymorph structures, which are generally classified as rhombic calcite, needle-like aragonite and spherical vaterite. Calcite belonging to the trigonal-hexagonal-scalenohedral crystallographic class is the most stable phase at room temperature under normal atmospheric conditions, while aragonite and vaterite belong to the orthorombic-dipyramidal class and hexagonal-dihexagonal-dipyramidal class, respectively. The latter two are metastable polymorphs which readily transform into stable calcite. The specific formation of each of the polymorphs of crystalline calcium carbonate depends mainly on the precipitation conditions. Supersaturation is usually considered to be the main controlling factor.[14] Many experimental studies have been reported about the synthetic precipitation of the various forms of calcium carbonate and the conditions under which these may be produced, including the initial supersaturation, temperature, pressure, pH and hydrodynamics. The effect of impurities and additives has also been well studied.[15–29]

The formation of calcite ($CaCO_3$) and elemental selenium (Se^0) entails complex processes, and numerous studies have been reported in the literature. The coexistence and the simultaneous precipitation/growth of these solid structures, however, have not been studied and/or reported to our knowledge. In this study, the hydrothermal carbonation of calcium hydroxide under high CO_2−Ar pressure (90 bar) coupled with a complex selenocystine fragmentation under O_2-poor and O_2-rich conditions was carried out by using a semibatch system (sampling with time) in order to synthesize elemental selenium (Se^0)/calcite composites.

Several analytical techniques were used to characterize selected solid samples (SEM/EDS, TEM/EDS, XRD and

* Corresponding author: German Montes-Hernandez. E-mail: german.montes-hernandez@obs.ujf-grenoble.fr; german_montes@hotmail.com.
† LGIT, University Joseph Fourier, Observatoire de Grenoble and CNRS.
‡ Institut Laue-Langevin.
§ LGCA, University Joseph Fourier, Observatoire de Grenoble and CNRS.
|| Physics of Geological Processes, University of Oslo.
⊥ Institute of Radiochemistry, FZD.
The Rossendorf Beamline at ESRF.
▽ LCABIE, IPREM, UMR CNRS 5254, Université de Pau et des Pays de l'Adour.

10.1021/cg800141p CCC: $40.75
Published on Web 05/28/2008

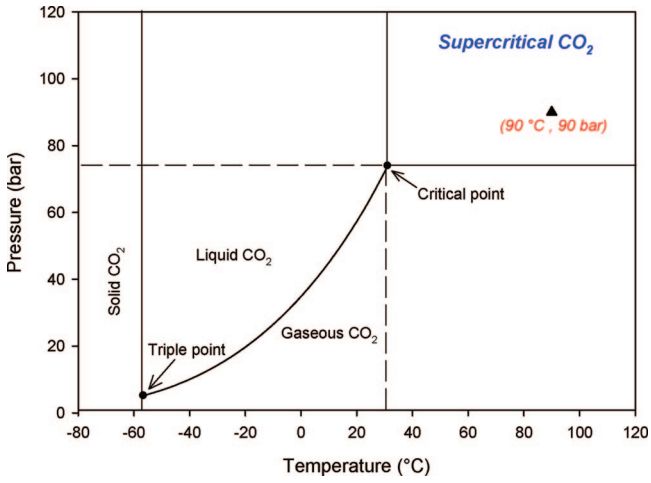

Figure 1. Experimental $P-T$ conditions represented on a pressure−temperature phase diagram for CO_2.

XANES and EXAFS spectroscopy) and selected solution samples (ICP/AES and HPLC/ICPMS).

2. Materials and Methods

2.1. Synthesis of Se^0/Calcite Composite. (a) O_2-Poor Conditions/Purge Step. One liter of high-purity water with an electrical resistivity of 18.2 MΩ·cm, 3 g of commercial portlandite $Ca(OH)_2$ (calcium hydroxide provided by Sigma-Aldrich) with 96% chemical purity (3% $CaCO_3$ and 1% other impurities) and different quantities (0, 50, 100 or 200 mg) of seleno-L-cystine $CO_2HCH(NH_2)CH_2(Se)_2CH_2CH(NH_2)CO_2H$ (provided by Sigma-Aldrich) with chemical purity ≥98.0% were placed in a titanium reactor (Parr autoclave with internal volume of 2 L). The hydroxide and selenocystine particles were immediately dispersed by mechanical agitation (400 rpm). Then, at room temperature the argon gas with 99.999% chemical purity (provided by Linde Gas S.A.) was injected into the reaction cell in order to control the pressure at 90 bar during 30 min. After this time period, the suspension was heated to 90 °C with a furnace adapted to the reactor. During this heating stage the pressure increased into the system because the gas pressure is a function of temperature ($P = f(T)$), but it was maintained constant at 90 bar by successive manual purge until the temperature was stabilized after 90 min. Then, about 20 mL of suspension was sampled in the reactor ($t = 0$), and immediately a flash purge was carried out until atmospheric pressure was reached. Due to the argon sorption in the suspension, the heating stage and the gas purge, dissolved oxygen was partially removed (O_2-poor conditions). However, the oxygen concentration inside the reaction cell could not be monitored. When the atmospheric pressure was reached in the reactor, 14.5 g of CO_2 with 99.995% chemical purity (provided by Linde Gas S.A.) was injected in the reactor and the total pressure in the system was immediately adjusted to 90 bar by argon injection. At these T and P conditions, the vapor phase consists mainly of an Ar + CO_2 mixture with CO_2 in supercritical state (see Figure 1). About 20 mL of suspension was sampled in the reactor as a function of time (t = 2, 6, 10, 30 and 60 min) during composite formation.

At the end of the experiment, the reaction cell was rapidly depressurized (1 min) during the water cooling from 90 to 35 °C (15 min). The autoclave was disassembled, and the solid product was recovered by centrifugation (30 min at 12,000 rpm) and decanting the supernatant solutions. Finally, the solid product was dried in the centrifugation flasks for 72 h at 65 °C, manually recovered and stocked in plastic flasks.

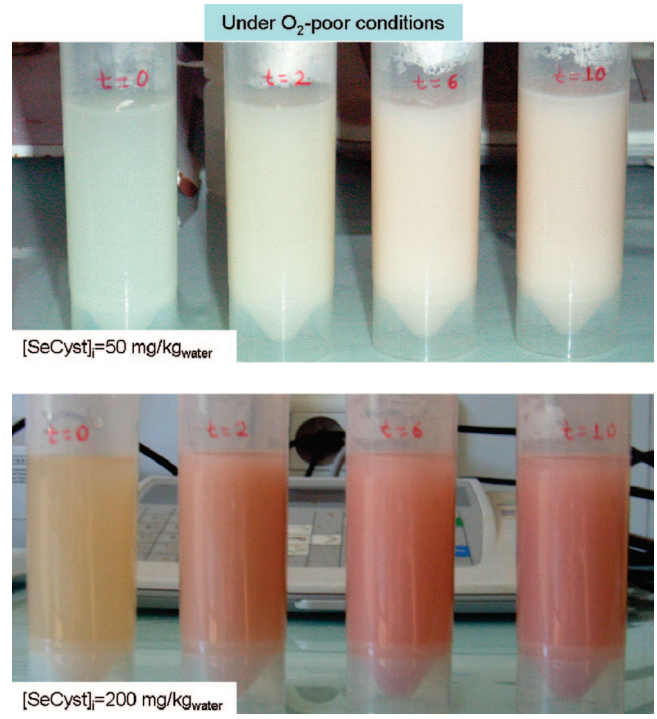

Figure 2. Coloration change of Se^0/calcite composite at different selenocystine doses and under O_2-poor conditions. Note that the Se^0/calcite composite was manually dispersed to take these photographs.

(b) O_2-Rich Conditions/No Purge Step. For these experiments, the dispersions (water−calcium hydroxide−selenocystine, composition as described above) were heated to 90 °C at atmospheric pressure. When the temperature was stable, about 20 mL of suspension was sampled in the reactor ($t = 0$). Then, 14.5 g of CO_2 was injected into the reactor, and the total pressure in the system was immediately adjusted to 90 bar by argon injection. After the pressure setting, sampling and composite recovery procedures were applied as described above for the O_2-poor system.

A total of eight experiments was carried out, four under O_2-poor conditions and four under O_2-rich conditions. For each experiment, six suspension samples were withdrawn from the reactor. In addition, the experiments with 200 mg of selenocystine under O_2-poor and O_2-rich conditions were repeated three times in order to check their color reproducibility.

2.2. Composite Characterization. (a) Macroscopic Observations. The coloration change with reaction time was imaged by using a charge-coupled device camera (RICOH, Caplio R1v, 5.0 M pixels 4.8× wide zoom).

(b) Microscopic Observations and Microstructure Characterization. Morphological analyses of five selected composite solid samples were performed by scanning electron microscopy (SEM), using a HITACHI S-4800 microscope. Isolated fine particles (oriented on carbon Ni grids) of the selected composite samples were also studied using a JEOL 3010 transmission electron microscope (TEM) equipped with an energy dispersive X-ray analyzer (EDS) to image the morphology of the particles and to identify the elemental composition of the precipitates.

The starting materials ($Ca(OH)_2$ and selenocystine) and four selected composite samples were characterized by X-ray powder diffraction using a Kristalloflex 810, SIEMENS diffractometer in Bragg−Brentano geometry. The XRD patterns were collected

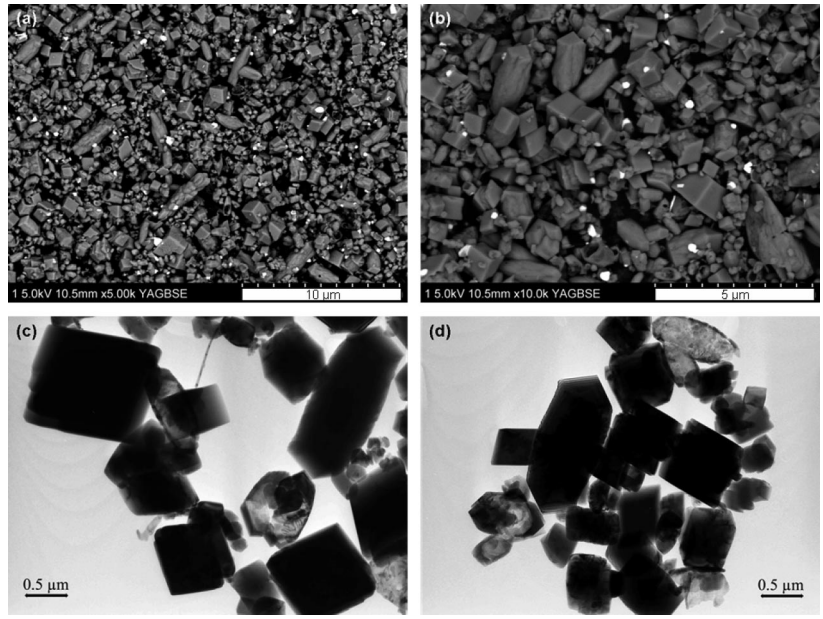

Figure 3. Red Se^0/calcite composite synthesized by hydrothermal carbonation of calcium hydroxide coupled with a complex selenocystine fragmentation under O_2-poor conditions. (a and b) Backscattering SEM observations "without metal coating". (c and d) TEM micrographs.

using Co $K\alpha_1$ ($\lambda_{K\alpha1} = 1.7889$ Å) and $K\alpha_2$ ($\lambda_{K\alpha2} = 1.7928$ Å) radiation in the range $2\theta = 5-80°$ with a step size of 0.02° and a counting time of 8 s per step. Rietveld refinements on the XRD patterns of the obtained pure calcite and composites were performed using the FULLPROF package.[30] Models to characterize the coherent domain sizes and the strain within the calcite crystallites were applied following the procedure described by Montes-Hernandez et al.[31]

The selenocystine powder and three selected composite samples (water-saturated wet pastes) were also characterized by XANES and EXAFS spectroscopy. X-ray absorption near-edge (XANES) and extended X-ray absorption fine-structure (EXAFS) spectra were collected at the Rossendorf Beamline at ESRF (Grenoble, France) using a 13-element high-purity germanium detector (Canberra) together with a digital signal processing unit (XIA) for fluorescence detection. For energy calibration, a gold foil (K-edge at 11919 eV) was chosen because of its greater inertness and hence reliability in comparison to Se. With this approach, we determined an edge energy of 12656 eV for trigonal Se, instead of the tabulated value of 12658 eV for zerovalent Se. Dead time correction of the fluorescence signal, energy calibration and the averaging of single scans, as well as linear combination fits were performed with the software package SixPack. Shell fitting was done in WinXAS.

2.3. Physicochemical characterization of aqueous solutions. (a) Total element concentration and pH. Ten milliliters for all sampled suspensions were filtered through a 0.22 μm pore-size filter, and the obtained aqueous solutions were immediately acidified with a nitric acid solution and stored at 4 °C for further measurement of [Ca] and [Se] by inductively coupled plasma atomic emission spectrometry (ICP Perkin-Elmer Optima 3300 DV). The pH was also systematically measured at 25 °C by using a MA235 pH/ion analyzer in filtered solutions without acidification. Note that the pH measurement was carried out at 25 °C after filtration, cooling and degasification of the solutions. While this measurement is not representative of in situ pH, it provides a reasonable estimate of the solution saturation index at standard conditions (25 °C and 1 atm).

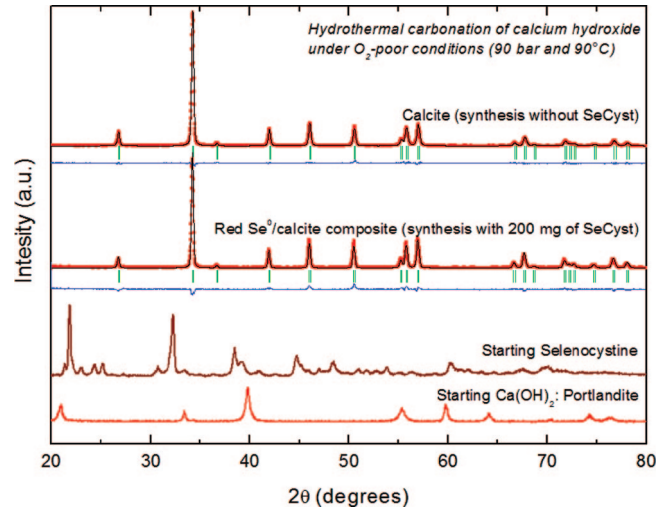

Figure 4. XRD patterns of starting solid materials (calcium hydroxide and selenocystine) and solid products (pure calcite and red Se^0/calcite composite). Results of the Rietveld refinements of the pure calcite and of the Se^0/calcite composite are presented; red points, experimental; black line, Rietveld refined model; blue line, difference; green lines, positions of Bragg peaks. Hydrothermal carbonation of calcium hydroxide under O_2-poor conditions ($P = 90$ bar; $T = 90$ °C; $Ca(OH)_2$ dose = 3 g/kg_{water}; selenocystine dose = 200 mg/kg_{water}; 1 h of reaction time).

(b) Selenium Speciation. Ten milliliters of each of the twelve sampled suspensions were filtered through a 0.22 μm pore-size filter, and the obtained aqueous solutions were immediately stored at 4 °C for further measurement (after one week). Selenocystine (SeCyst), selenomethionine (SeMet), selenite (Se(IV)) and selenate (Se(VI)) were measured by liquid chromatography coupled with ICPMS detection (HPLC/ICPMS) as previously described.[32] Briefly, chromatographic separation was carried out using an Agilent 1100 series HPLC pump, equipped with an autosampler and variable volume sample loop. The analytical column was a Hamilton PRP-X-100, 10 μm particle size, 25 cm length × 4.1 mm internal diameter. The chromatographic separation of the four sele-

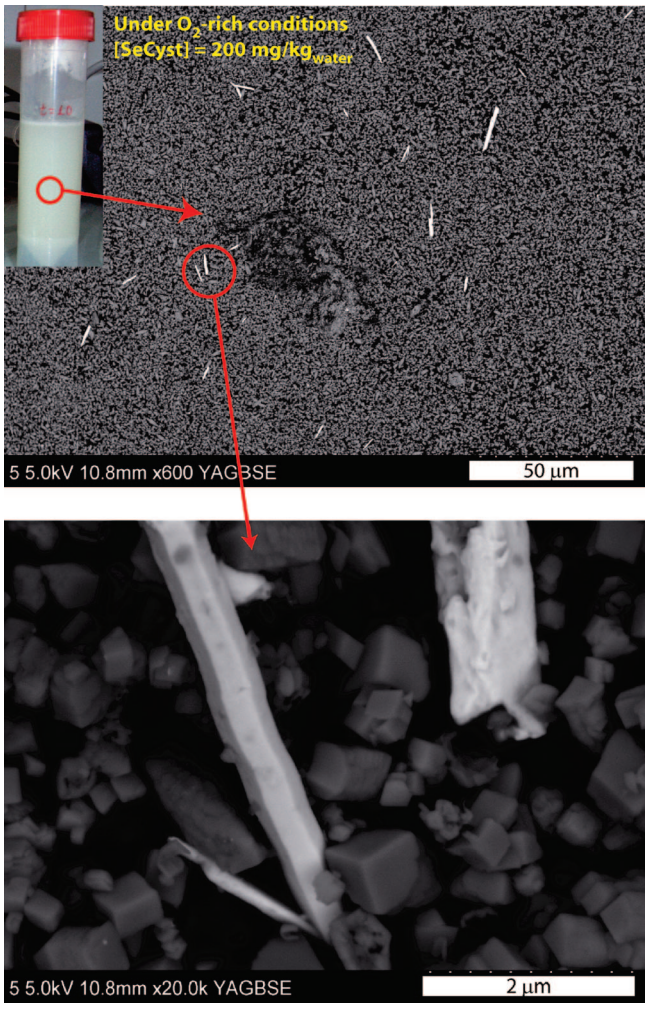

Figure 5. Gray Se^0/calcite composite synthesized by hydrothermal carbonation of calcium hydroxide coupled with a complex selenocystine fragmentation under O_2-rich conditions. Backscattering SEM observations "without metal coating".

nium species was obtained using a 5 mmol L^{-1} ammonium citrate buffer at pH 5.2. Injection volume was fixed at 100 μL. Methanol (2% v/v) was added in the mobile phase to improve sensitivity. The mobile phase was delivered at 1 mL min^{-1} isocratically. The HPLC−ICPMS interface consisted of a polyetheretherketone (PEEK) tube. Selenium selective detection was performed with an Agilent 7500ce ICPMS equipped with a collision reaction cell. The instrumental and acquisition parameters were as follows: radiofrequency power (1500 W); carrier gas (1 L/min); reaction cell gas (H_2 at 5.0 mL/min). Integration time was 0.4 s for both *m*/*z* 77 and 78. Selenium species were quantified in diluted samples (1/10000) by external calibration with standard solutions of the respective pure compounds. Quantification was performed with selenium isotope *m*/*z* 78.

3. Results and Discussion

3.1. Characterization of Se^0/Calcite Composite Produced under O_2-Poor Conditions. Macroscopically, the typical color of calcite is white, while the typical colors of Se^0 are gray (hexagonal Se) or red (amorphous and alpha-monoclinic Se). In the current study, a red composite was produced under O_2-poor conditions. The red coloration depended on the selenocystine dose; reddish hues started to be observable from 50 mg/

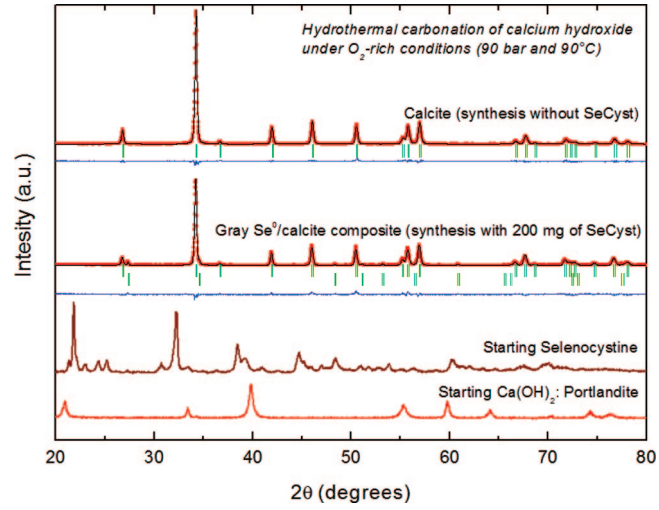

Figure 6. XRD patterns of starting solid materials (calcium hydroxide and selenocystine) and solid products (pure calcite and gray Se^0/calcite composite). Results of the Rietveld refinements of the pure calcite and of the gray Se^0/calcite are presented. Two crystalline phases can be discerned: pure calcite (first line of green lines) and the hexagonal Se^0. Red points: experimental. Black line: Rietveld refined model. Blue line: difference. Green lines: positions of Bragg peaks. Hydrothermal carbonation of calcium hydroxide under O_2-rich conditions (P = 90 bar; T = 90 °C; $Ca(OH)_2$ dose = 3 g/kg_{water}; selenocystine dose = 200 mg/kg_{water}; 1 h of reaction time).

kg_{water} on, and the color intensity increased with an increasing selenocystine dose (Figure 2). This coloration behavior was reproducible at a constant calcium hydroxide dose (3 g/kg_{water} for this study). The coloration of composite was stable in its mother aqueous solution even after several weeks of storage at room conditions and without further protection from light.

Microscopically, the red composite was mainly composed of spherical selenium nanoparticles (<500 nm) deposited on the calcite matrix. The carbonate matrix consisted of nanometer and micrometer-sized rhombohedral crystal (<2 μm) and agglomerates and/or aggregates in the micrometer range (<5 μm) (Figure 3). An average coherent domain size of $\langle d \rangle_{red}$ = 372 ± 100 nm was estimated using Rietveld refinement of XRD patterns.

X-ray diffraction suggests a complete $Ca(OH)_2$−calcite conversion, i.e., that the metastable crystalline phases of $CaCO_3$, such as vaterite and aragonite were not produced during the $Ca(OH)_2$ carbonation process. Selenocystine, which is a crystalline organic material, could not be detected anymore by X-ray diffraction spectra (Figure 4). This suggests that selenocystine was completely dissolved and/or completely transformed into red Se^0 nanoparticles (observed by SEM and TEM microscopy). However, these results do not provide any information on the selenocystine fragmentation mechanism. Note that red spherical Se^0 nanoparticles could not be identified by X-ray powder diffraction due to their poor crystallinity, suggesting an X-ray amorphous state.

3.2. Characterization of Se^0/Calcite Composite Produced under O_2-Rich Conditions. During these experiments, a gray composite was formed. The gray color intensity slightly increased with selenocystine dose from 50 to 200 mg/kg_{water}. As for the O_2-system, the composite coloration was stable in its mother aqueous solution even after several weeks of storage at room conditions and without protection from light. Microscopic observations showed that the composite consisted of rod-shaped hexagonal selenium microparticles (<25 μm) dispersed in the nanosized calcite matrix (Figure 5). An average coherent domain size of $\langle d \rangle_{gray}$ = 156 ± 86 nm was

determined by Rietveld refinements of the XRD data. SEM observations (Figure 5) reveal microscopic aggregates (<1 μm).

Concerning the rod-shaped hexagonal selenium, the X-ray diffraction measurements support these microscopic observations. It is well-known that the trigonal or hexagonal morphologies are the most stable crystalline phases for Se^0. Even at the small concentration, the gray well-crystallized elemental selenium in a given composite could be identified by the X-ray diffraction (Figure 6). This figure also demonstrates the complete $Ca(OH)_2$−calcite conversion under O_2-rich conditions, revealing that the oxygen had not a significant effect on the efficiency of the carbonation process. However, the available quantity of oxygen in the suspension controls the chemical transformation (or chemical fragmentation) of the selenocystine, causing the precipitation/growth of elemental selenium with two different structures and particle sizes.

3.3. Precipitation/Growth of Calcite with Unusual Morphologies. For our experiments, the hydrothermal carbonation of calcium hydroxide described by the global reaction,

$$Ca(OH)_{2(s)} + CO_{2(aq)} \rightarrow CaCO_{3(s)} + H_2O$$

is an exothermic process involving simultaneously the dissolution of $Ca(OH)_2$,

$$Ca(OH)_{2(s)} \xrightarrow{\text{water}} Ca^{2+} + 2OH^-$$

and the dissociation of aqueous CO_2,

$$CO_{2(aq)} + H_2O \rightarrow CO_3^{2-} + 2H^+$$

These two coupled reactions rapidly produce a supersaturation (S_I) of the solution with respect to calcite,

$$S_I = \frac{(Ca^{2+})(CO_3^{2-})}{K_{sp}} > 1$$

where (Ca^{2+}) and (CO_3^{2-}) are the activities of calcium and carbonate ions in the solution, respectively, and K_{sp} is the thermodynamic solubility product of calcite. Then, the nucleation stage (formation of nuclei or critical cluster) takes place in the system,

$$Ca^{2+} + CO_3^{2-} \rightarrow CaCO_3(\text{nuclei})$$

The sampling of the suspensions in the reactor at different times allowed the identification of the nucleation stage, characterized by the formation of an apparent stable emulsion after about two minutes of reaction time.

Finally, the crystal growth occurred spontaneously until the equilibrium between calcite and its solution was reached,

$$CaCO_3(\text{nuclei}) \rightarrow CaCO_3(\text{calcite})$$

In this study, the selenocystine fragmentation during the heating and carbonation process had an insignificant effect on the $Ca(OH)_2$−calcite conversion. In addition, the reactions kinetics reflected by ex situ pH and Ca concentration in solutions was

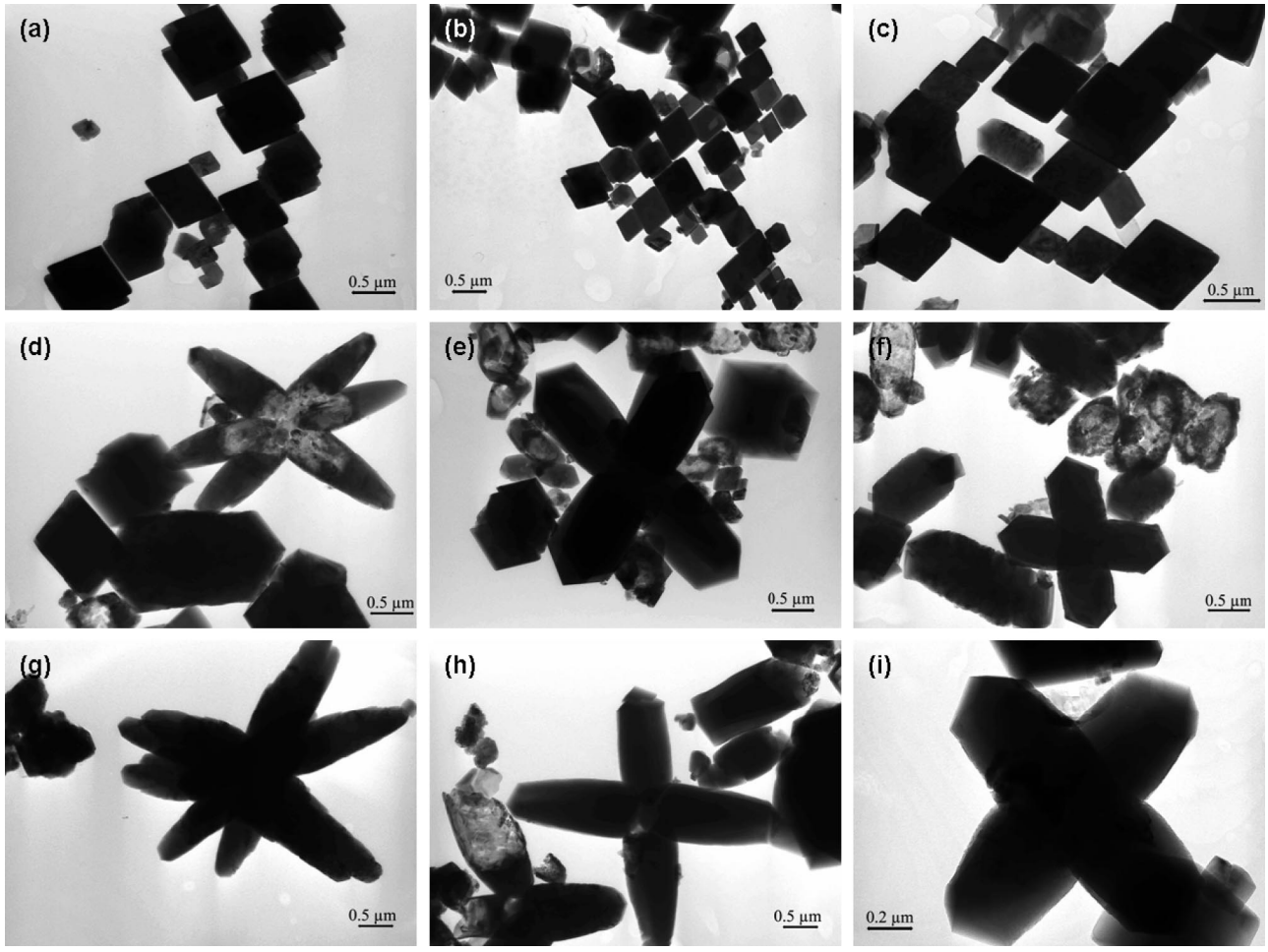

Figure 7. (a, b and c) Rhombohedral nano- and microparticles of calcite for a hydrothermal $Ca(OH)_2$ carbonation process without initial selenocystine dose. (d, e, f, g, h and i) Morphology of calcite particles for a hydrothermal $Ca(OH)_2$ carbonation process with initial selenocystine dose (200 mg/kg_{water}).

Table 1. Selenium Solution Speciation by HPLC/ICPMS under Two Hydrothermal Carbonation−Selenocystine Fragmentation Regimes[a]

				t_R, min			
t, min	SeCyst	SeIV	SeVI	2.80	5.91	7.03	$pH_{25°C}$
	O_2-Poor Conditions and 200 mg/kg_{water} of Selenocystine						
0	0.86 ± 0.08	24 ± 1	nd	ni		ni	12.60
2	nd	9.1 ± 0.7	nq		ni		12.43
6	8.9 ± 0.4	0.37 ± 0.01	nq		ni		7.44
10	9.3 ± 0.1	0.95 ± 0.02	nd		ni		7.30
30	4.0 ± 0.2	1.7 ± 0.2	nq		ni		7.34
60	nd	2.5 ± 0.1	nd				7.10
	O_2-Rich Conditions and 100 mg/kg_{water} of Selenocystine						
0	nd	17 ± 1	0.21 ± 0.02	ni	ni		12.63
2	nd	4.7 ± 0.2	0.27 ± 0.01		ni		12.58
6	0.68 ± 0.05	1.5 ± 0.1	0.22 ± 0.2				8.03
10	0.65 ± 0.05	4.0 ± 0.3	0.27 ± 0.02				7.30
30	0.15 ± 0.03	5.6 ± 0.2	0.25 ± 0.02				7.28
60	nd	5.7 ± 0.3	0.24 ± 0.02				7.15

[a] Concentrations given in mg (Se) L^{-1}. *t*: reaction time ($t = 0$ at CO_2 injection). SeCyst: seleno-L-cystine. SeIV: selenite (SeO_3^{-2}). SeVI: selenate (SeO_4^{-2}). t_R: retention time of HPLC/ICPMS measurements. $pH_{25°C}$: pH measured at 25°C. nd: not detected. nq: not quantifiable. ni: not identifiable.

very similar for all experiments. However, several TEM micrographs revealed an unusual agglomeration/aggregation process of rhombohedral particles, leading to an unusual, star-like morphology of carbonate particles (see Figure 7). The microscopic observations suggest that the star-like morphologies correspond to a physical aggregation of the crystalline nanoparticles. This observation was further supported by the fact that the stars could be disassembled by a relatively weak physical force by gently grinding the composite in a mortar in the presence of ethanol (not shown). Therefore, the formation of nanoparticles can be explained by the classic theory of crystal growth inhibition; the surface of calcite nuclei was poisoned by adsorption/incorporation of selenite (SeO_3^{-2}) and other unidentified impurities produced in situ during the selenocystine chemical fragmentation (see Table 1 and subsection 3.4). In addition, preliminary experimental results, not shown here, suggest that the incorporation of selenite (SeO_3^{-2}) into calcite retards the CO_2 transfer in the suspension during the $Ca(OH)_2$ carbonation process.

It is well-known that impurities and additives in the solution can modify crystal habits and induce crystallographic twinning by sorption of the impurities or additives to the growing crystal surfaces, thereby altering the growth kinetics. Recently, in situ observations revealed that polyaspartate induces liquid−liquid phase separation of droplets of a mineral precursor. The droplets deposit on the substrate and coalesce to form a coating, which then solidifies into calcitic tablets and films. Transition bars form during the amorphous to crystalline transition, leading to the sectorization of calcite tablets. The defect textures and crystal morphologies are atypical of solution grown crystals.[33–36]

3.4. Selenocystine Chemical Fragmentation. Selenocystine powder is slightly soluble in pure water at atmospheric conditions, thereby increasing the solution pH from 5.8 to about 8.5 at atmospheric conditions due to the high proton (H^+) affinity of the two amine groups. By liquid chromatography coupled to ICPMS detection, it was demonstrated that selenocystine molecules are conserved during several weeks in HCl acidic solution (pH = 1) and preferentially at high selenocystine concentration (1 g(Se)/L).

In contrast, selenocystine was rapidly transformed in $Ca(OH)_2$ alkaline solutions (pH ≅ 12.5 measured at 25 °C). Under these conditions, about 25% of the initial selenium contained in the

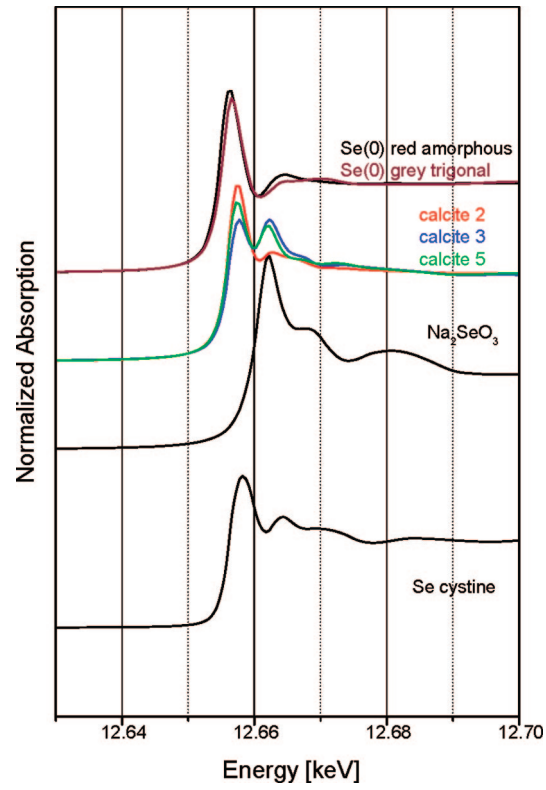

Figure 8. Se K-edge XANES of three calcite samples in comparison to select references. Calcite 2: experiment under O_2-poor conditions, 100 mg/kg_{water} of selenocystine, 1 h of reaction. Calcite 3: experiment under O_2-poor conditions, 50 mg/kg_{water} of selenocystine, 1 h of reaction. Calcite 5: experiment under O_2-rich conditions, 100 mg/kg_{water} of selenocystine, 1 h of reaction. Se cystine corresponds to the selenocystine reference.

selenocystine (experiment with 200 mg/kg_{water}) was oxidized to Se(IV) under O_2-poor conditions. At the O_2-rich conditions employed during our experiment, even about 40% of initial selenium (experiment with 100 mg/kg_{water}) was oxidized predominately to Se(IV) and a minor amount to Se(VI) (Table 1). This partial oxidation of selenocystine took place before the carbonation process, i.e. before the injection of CO_2 in the reactor ($t = 0$). This confirms the instability of selenocystine in alkaline solutions, controlled by the initial selenocystine dose and the amount of dissolved oxygen.

The production of selenite oxyanions during the carbonation process follows a complex path. Initially, the selenite solution concentration drastically decreased by adsorption on incorporation into the calcite matrix, perturbing the crystal growth and particle aggregation process of calcite (3.3 and Figure 7). Subsequently, selenite solution increased with slow kinetics, caused by the dissolution of fine particles of calcite due to excess of CO_2 in the system.

The adsorption on and/or incorporation of selenite (SeO_3^{-2}) into the calcite was supported by XANES and EXAFS spectrometry. This powerful technique allowed also the identification and quantification of different selenium forms in coexistence with calcite for three selected solid samples (labeled calcite 2, calcite 3 and calcite 5 in Figures 8 and Figure 9.

The Se K-edge XANES spectra of the three calcite samples are dominated by a white line at 12,656.5 eV, indicative of elemental Se (Figure 8).[37,38] Since the white line peak position of selenocystine is about 2 eV above that of elemental Se, we can discard that substantial amount of selenocystine was present in the samples. Samples 3 and 5 have an additional strong

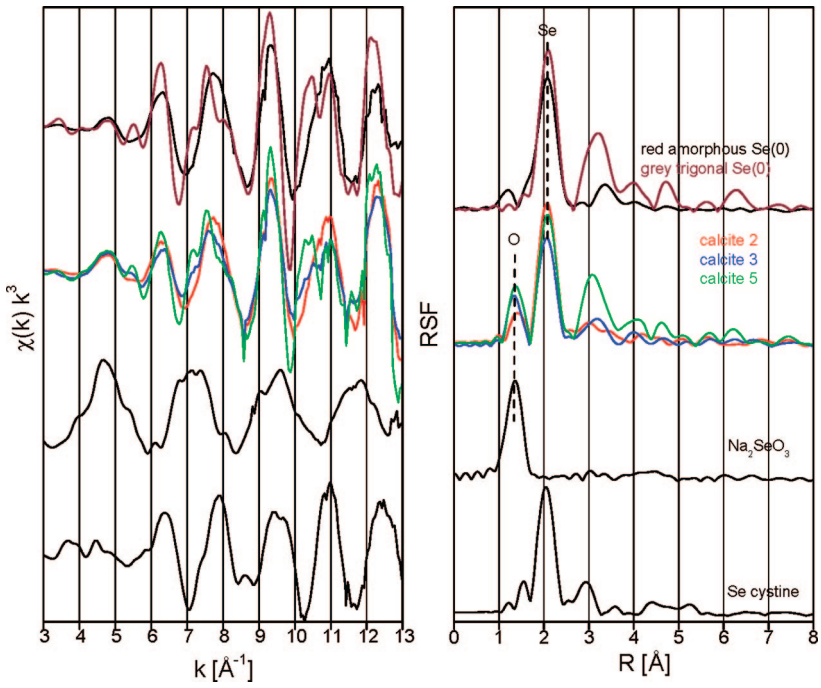

Figure 9. Se K-edge EXAFS spectra (left) and corresponding Fourier transforms (right) of the three calcite samples and select references. Calcite 2: experiment under O_2-poor conditions, 100 mg/kg_{water} of selenocystine, 1 h of reaction. Calcite 3: experiment under O_2-poor conditions, 50 mg/kg_{water} of selenocystine, 1 h of reaction. Calcite 5: experiment under O_2-rich conditions, 100 mg/kg_{water} of selenocystine, 1 h of reaction. Se cystine corresponds to the selenocystine reference.

Table 2. Linear Combination Fit of k^3-Weighted EXAFS Spectra[a]

sample	Se gray	Se red	Se(IV)	sum
calcite 2	0.02	0.87	0.12	1.01
calcite 3	0.15	0.50	0.28	0.93
calcite 5	0.74	0.07	0.23	1.04

[a] Calcite 2: experiment under O_2-poor conditions, 100 mg/kg_{water} of selenocystine, 1 h of reaction. Calcite 3: experiment under O_2-poor conditions, 50 mg/kg_{water} of selenocystine, 1 h of reaction. Calcite 5: experiment under O_2-rich conditions, 100 mg/kg_{water} of selenocystine, 1 h of reaction. Se(IV) correspond to $Se(IV)_{aquo}$ and Na_2SeO_3 references in Charlet et al..[38]

oscillation at 12,662 eV, which coincides with the white line of Se(IV), indicating that these samples contain tetravalent Se in addition to elemental Se.

The corresponding Se K-edge EXAFS revealing structural features are shown in Figure 9. The Fourier transform peaks at about 2.1 Å (uncorrected for phase shift) in the spectra of elemental Se and of selenocystine are due to Se−Se backscattering within the coordination sphere. This is also the strongest peak in the Fourier transform spectra of the three calcite samples. Red and gray elemental Se are discernible by the intensity of the first and second shells, the ones for gray Se being much stronger due to the higher structural order. The spectrum of sample 5 is very similar to that of gray Se, while samples 2 and 3 are closer to red Se. The Se−O backscattering peak of the Se(IV) reference, Na_2SeO_3, occurs at a smaller distance of 1.4 Å. All three sample spectra show a contribution from this shell, although much lower in intensity than the pure Se(IV) compound. We can therefore conclude that all samples contain a small amount of Se(IV) adsorbed/incorporated onto/into calcite in addition to Se(0). This is in agreement with XANES results.

To further support this tentative phase identification and to derive quantitative information, we performed linear combination fits of the k^3-weighted EXAFS spectra (Table 2). In confirmation of the visual interpretation of EXAFS spectra, sample calcite 5 contains a large amount of gray Se, while the other two samples are dominated by red Se. Note that satisfying fits were achieved only when a reference spectrum of the aqueous selenite was added for samples calcite 2 and calcite 3, and the reference spectrum of the Se(IV) solid phase was added for sample calcite 5. The relative amount of Se(IV) corresponds to the relative height of the Se−O Fourier peak (Figure 9).

The time-lapse sampling in the reactor and the use of a multitechnique approach give relevant information on the chemical fragmentation of selenocystine in our experiments. However, it is still difficult to propose an unequivocal chemical reaction mechanism. Note for example, that three transient selenium species could not be identified and quantified by HPLC/ICPMS (Table 1), because only four selenium references were available for this study.

4. Conclusion

The main purpose of our study was to synthesize a Se^0/calcite composite. The synthesis was successfully performed by using the hydrothermal carbonation of calcium hydroxide under high CO_2−Ar pressure (90 bar) and high temperature (90 °C) coupled to a complex selenocystine fragmentation process under both O_2-poor and O_2-rich conditions. Under O_2-poor conditions (i.e., with purge stage), the composite contained Se mainly in the form of spherical Se^0 nanoparticles (<500 nm) deposited on the calcite matrix, causing a stable red coloration. In contrast, under O_2-rich conditions (i.e., without purge stage), the composite contained rod-shaped hexagonal Se^0 microparticles (<25 μm) dispersed in the calcite matrix, causing a stable gray coloration. The carbonate matrix for both systems was constituted by nano- and microrhombohedral crystals (<2 μm) and micrometric agglomerates and/or aggregates (<5 μm).

It was also observed that the gas purge in the system and the selenocystine dose (mg/kg_{water}) play a crucial role on the selenocystine fragmentation mechanism during $Ca(OH)_2$ sus-

pension heating (at 90 °C) and carbonation stages, causing the precipitation/growth of elemental selenium with different morphologies and particle sizes. The selenocystine fragmentation influenced the precipitation/growth of calcite with unusual morphologies.

Finally, the synthesized composites could have a high potential for medical (e.g., dietary supplement) or industrial (e.g., pigments) applications. In addition, this study may have implications in the field of biomineralization.

Acknowledgment. The authors are grateful to the National Research Agency, ANR (GeoCarbone-CARBONATATION project), France, for providing the financial support for this work. J. Ganbaja, A. Kohler, D. Tisserand and N. Geoffroy are thanked for their technical help and assistance.

References

(1) Song, J. M.; Zhu, J. H.; Yu, S. H. *J. Phys. Chem. B.* **2006)** , *110*, 23790.
(2) Ding, Y.; Li, Q.; Jia, Y.; Chen, L.; Xing, J.; Qian, Y. *J. Cryst. Growth* **2002**, *241*, 489.
(3) Bai, Y.; Wang, Y.; Zhou, Y.; Li, W.; Zheng, W. *Mater. Lett.* **2007**. doi:10.1016/j.matlet.2007.11.098.
(4) Kapolna, E.; Shah, M.; Caruso, J. A.; Fodor, P. *Food Chem.* **2007**, *101*, 1398.
(5) Tarze, A.; Dauplais, M.; Grigoras, I.; Lazard, M.; Ha-Duong, N. T.; Barbier, F.; Blanquet, S.; Plateau, P. *J. Biol. Chem.* **2007**, *282* (12), 8759.
(6) Caputo, R.; Capone, S.; Della Greca, M.; Longobardo, L.; Pinto, G. *Tetrahedron Lett.* **2007**, *48*, 1425.
(7) Peng, D.; Zhang, J.; Liu, Q.; Taylor, E. W. *J. Inorg. Biochem.* **2007**, *101*, 1457.
(8) Spallholz, J. E.; Hoffman, D. J. *Aquat. Toxicol.* **2002**, *57*, 27.
(9) Stewart, M. S.; Spallholz, J. E.; Neldner, K. H.; Pence, B. C. *Free Radical Biol. Med.* **1999**, *26*, 42.
(10) Ochsenkuhn-Petropoulou, M.; Tsopelas, F. *Anal. Chim. Acta* **2002**, *467*, 167.
(11) Goh, K. H.; Lim, T. T. *Chemosphere* **2004**, *55*, 849.
(12) Munier-Lamy, C.; Deneux-Mustin, S.; Mustin, C.; Merlet, D.; Berthelin, J.; Leyval, C. *J. Environ. Radioact.* **2007**. doi: 10.1016/j.jenvrad.2007.04.001.
(13) Simonoff, M.; Sergeant, C.; Poulain, S.; Pravikoff, M. S. *C. R. Chim.* **2007**. doi: 10.1016/J.crci.2007.02.010.
(14) Han, Y. S.; Hadiko, G.; Fuji, M.; Takahashi, M. *J. Cryst. Growth* **2005**, *276*, 541.
(15) Moore, L.; Hopwood, J. D.; Davey, R. J. *J. Cryst. Growth* **2004**, *261*, 93.
(16) Westin, K. J.; Rasmuson, A. C. *J. Colloids Interface Sci.* **2005**, *282*, 370.
(17) Tsuno, H.; Kagi, H.; Akagi, T. *Bull. Chem. Soc. Jpn.* **2001**, *74*, 479.
(18) Fujita, Y.; Redden, G. D.; Ingram, J.; Cortez, M. M.; Ferris, G.; Smith, R. W. *Geochem. Cosmochem. A* **2004**, *68*, 3261.
(19) Freij, S. J.; Godelitsas, A.; Putnis, A. *J. Cryst. Growth* **2005**, *273*, 535.
(20) Gower, L. A.; Tirrell, D. A. *J. Cryst. Growth* **1998**, *191*, 153.
(21) Jonasson, R. G.; Rispler, K.; Wiwchar, B.; Gunter, W. D. *Chem. Geol.* **1996**, *132*, 215.
(22) Chrissanthopoulos, A.; Tzanetos, N. P.; Andreopoulou, A. K.; Kallitsis, J.; Dalas, E. *J. Cryst. Growth* **2005**, *280*, 594.
(23) Menadakis, M.; Maroulis, G.; Koutsoukos, P. G. *Comput. Mater. Sci.* **2007**, *38*, 522.
(24) Dousi, E.; Kallitsis, J.; Chrisssanthopoulos, A.; Mangood, A. H.; Dalas, E. *J. Cryst. Growth* **2003**, *253*, 496.
(25) Pastero, L.; Costa, E.; Alessandria, B.; Rubbo, M.; Aquilano, D. *J. Cryst. Growth* **2003**, *247*, 472.
(26) Lee, Y. J.; Reeder, R. *Geochem.Cosmochem. A* **2006**, *70*, 2253.
(27) Temmam, M.; Paquette, J.; Vali, H. *Geochem. Cosmochem. A* **2000**, *64*, 2417.
(28) Dalas, E.; Chalias, A.; Gatos, D.; Barlos, K. *J. Colloids Interface Sci.* **2006**, *300*, 536.
(29) Montes-Hernandez, G.; Renard, F.; Geoffroy, N.; Charlet, L.; Pironon, J. *J. Cryst. Growth* **2007**, *308*, 228.
(30) Rodríguez-Carvajal, J. In *Collected Abstracts of Powder Diffraction Meeting*; Galy, J., Ed.; Toulouse, France, 1990.
(31) Montes-Hernandez, G.; Fernandez-Martinez, A.; Charlet, L.; Tisserand, D.; Renard, F. *J. Cryst. Growth* **2008**. doi: 10.1016/j.jcrysgro.2008.02.012.
(32) Darrouzès, J.; Bueno, M.; Simon, S.; Pannier, F.; Potin-Gautier, M. *Talanta* **2007**. doi: 10.1016/j.talanta.2007.11.020.
(33) Gower, L. B.; Odom, D. J. *J. Cryst. Growth* **2000**, *210*, 719.
(34) Cheng, X.; Varona, P. L.; Olszta, M. J.; Gower, L. B. *J. Cryst. Growth* **2007**, *307*, 395.
(35) Cheng, X.; Gower, L. B. *Biotechnol. Prog.* **2006**, *22*, 141.
(36) Dai, L.; Douglas, A. P.; Gower, L. B. *J. Non-Cryst. Solids* **2007**. doi: 10.1016/j.jnoncrysol.2007.10.022.
(37) Scheinost, A. C.; Charlet, L. *Environ. Sci. Technol.* **2008**, 1984–1989.
(38) Charlet, L.; Scheinost, A. C.; Tournassat, C.; Greneche, J. M.; Gehin, A.; Fernandez-Martinez, A.; Coudert, S.; Tisserand, D.; Brendle, J. *Geochim. Cosmochim. Acta* **2007**, *71*, 5731.

CG800141P